



Fig-2 shows the control strategy which is used for the generation of reference currents. PI control scheme is used for the control of both active and reactive power flow into the grid. The active power control is done through the d-axis component of grid current and the reactive power control through the q-axis component of grid current. The d and q axis reference currents are calculated as per the equations 1 and 2 as shown below. The three phase grid currents  $I_a$ ,  $I_b$  and  $I_c$  are sensed and transformed to dq0 reference frame. Synchronization of the reference frame to the grid voltage is achieved by Phase Locked Loop (PLL) method [1]. The control voltages for the three phases Voltage Source Inverter are generated based on the errors in d axis and q axis currents through PI controllers. The PI controllers produce the control voltages for the inverter in d and q axis based on equations 3 and 4. The compensation terms are added to improve the transient response of the system.

$$I_{d (ref)} = K_p V_h + K_i \int V_h dt \text{ -----(1)}$$

$$I_{q (ref)} = K_p V_j + K_i \int V_j dt \text{ -----(2)}$$

$$V'_d = K_p I_h + K_i \int I_h dt \text{ -----(3)}$$

$$V'_q = K_p I_j + K_i \int I_j dt \text{ -----(4)}$$

Where  $I_h$  and  $I_j$  are the errors in d axis and q axis grid currents and  $K_p$ ,  $K_i$  are the proportional and integral gains of the PI controllers. The voltages  $V'_d$ ,  $V'_q$  are then transformed into a b c coordinates to get control voltages  $V_a$ ,  $V_b$  and  $V_c$  for the PWM inverter.

## 2. SIMULATION AND PERFORMANCE EVALUATION

To evaluate the performance of the system, the model is examined under various conditions. These conditions include steady-state and dynamic conditions analysis such as variation in grid voltage and fault conditions. In each case, the performance of the system is analyzed. DC link voltage is maintained constant; the minimum value of dc reference voltage is determined by the inverter output voltage as

$$V_{dc (ref)} = 2 \times \sqrt{\frac{2}{3}} V_{g-line}$$

where  $V_{g-line}$  is the line to line voltage at the inverter output.

Fig- 3 shows the steady-state analysis of the system in which we can see that the system reaches steady-state after 2.5s.

Fig- 4 shows the effect on the system when 25% dip in grid voltage occurs between 4.5s to 5.5s. Active power reference is set at 2 MW and reactive power reference is set at zero. During the voltage dip, distortion in grid current occurs, and thus distortions are seen in active and reactive power. When distortion in grid voltage is cleared the active and reactive power follow the respective references. It also shows the effect on dc link voltage and voltage and current at the point of common coupling.

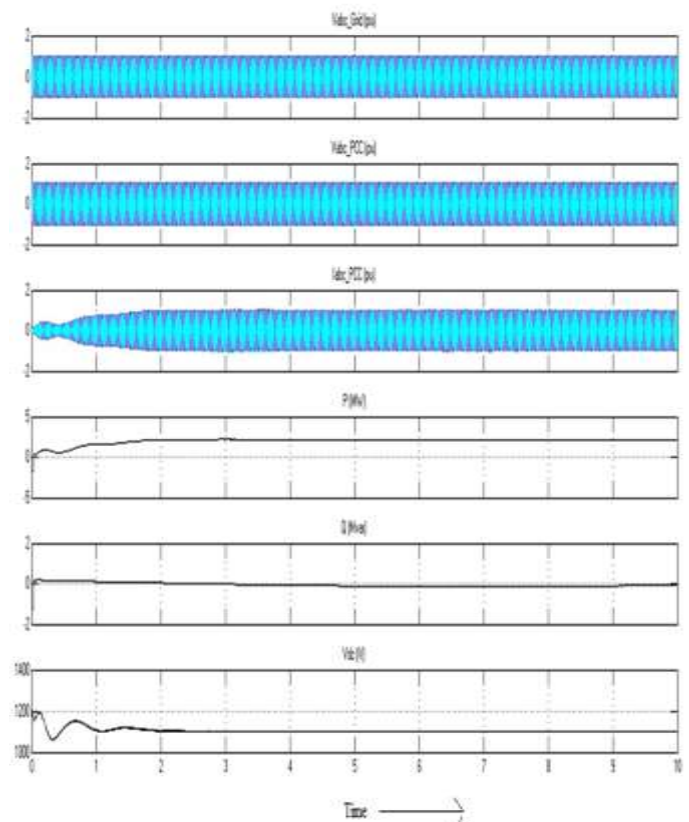


Fig -3: Steady-state analysis

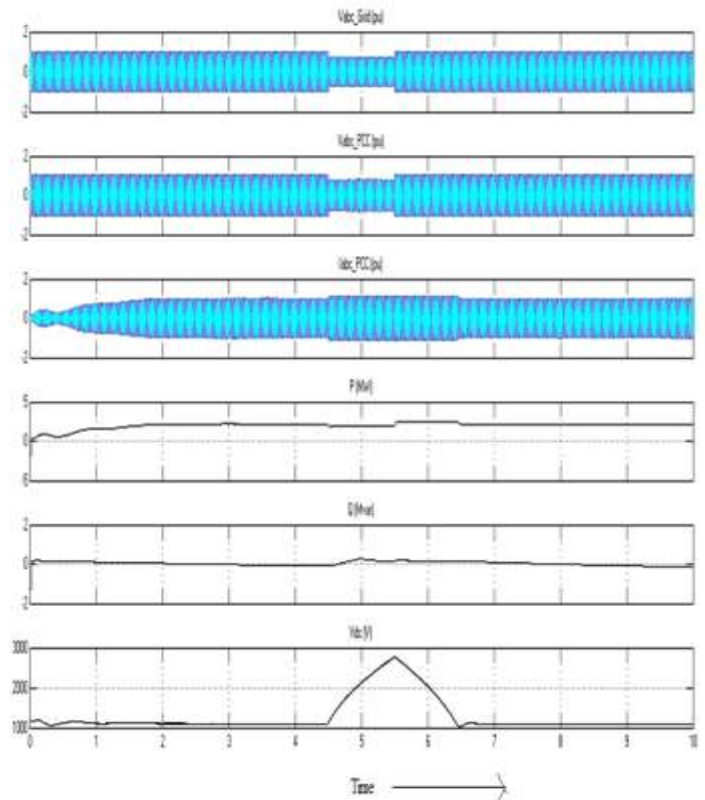
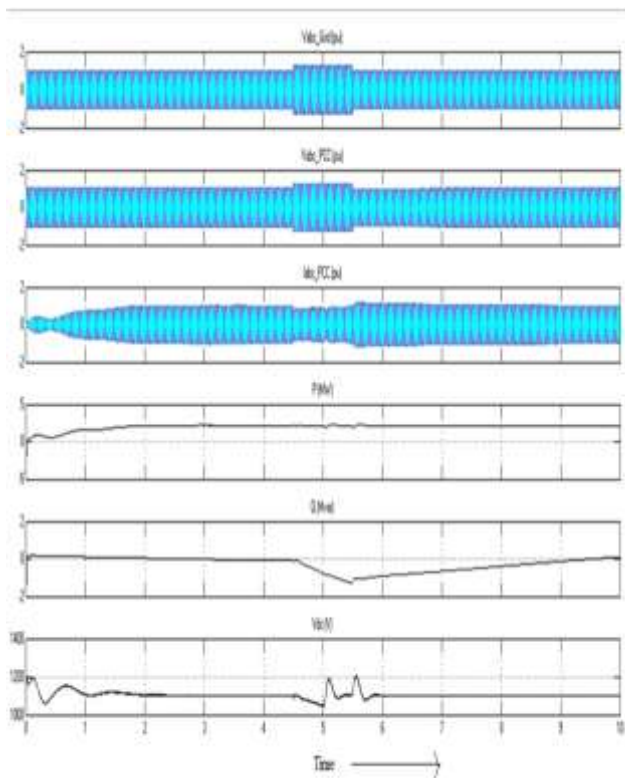


Fig -4: Dynamic analysis of the system for 25% dip in grid voltage.



**Fig -5:** Dynamic analysis of the system for 25% rise in grid voltage.

**Fig -5** shows the effect on the system when 25% rise in grid voltage imposed between time  $t= 4.5s$  and cleared at  $t= 5.5s$ . Active power reference is set at 2 MW and reactive power reference is set at zero. During the voltage rise, distortion in grid current occurs, and thus distortions are seen in active and reactive power. When distortion in grid voltage is cleared the active and reactive power follow the respective references. It also shows the effect on dc link voltage and voltage and current at the point of common coupling.

**Fig -6** shows the response of the system the under single line to a ground fault condition. Fault occurs at  $t = 4s$  and cleared at  $t = 5s$ . Active power reference is set at 2 MW and reactive power reference is set at zero. During the fault, distortion in grid current occurs, and thus distortions are seen in active and reactive power. When the fault is cleared the active and reactive power follow the respective references. It also shows the effect of a single line to ground fault on dc link voltage and voltage and current at the point of common coupling.

**Fig -7** shows the response of the system under line to line fault condition. The fault occurred at  $t = 4s$  and cleared at  $t = 5s$ . Active power reference is set at 2 MW and reactive power reference is set at zero. During fault distortion in grid current occurs, and thus distortions are seen in active and reactive power. When fault is cleared the active and reactive power follow the respective references. It also shows the effect of line to line fault on dc link voltage and voltage and current at the point of common coupling.

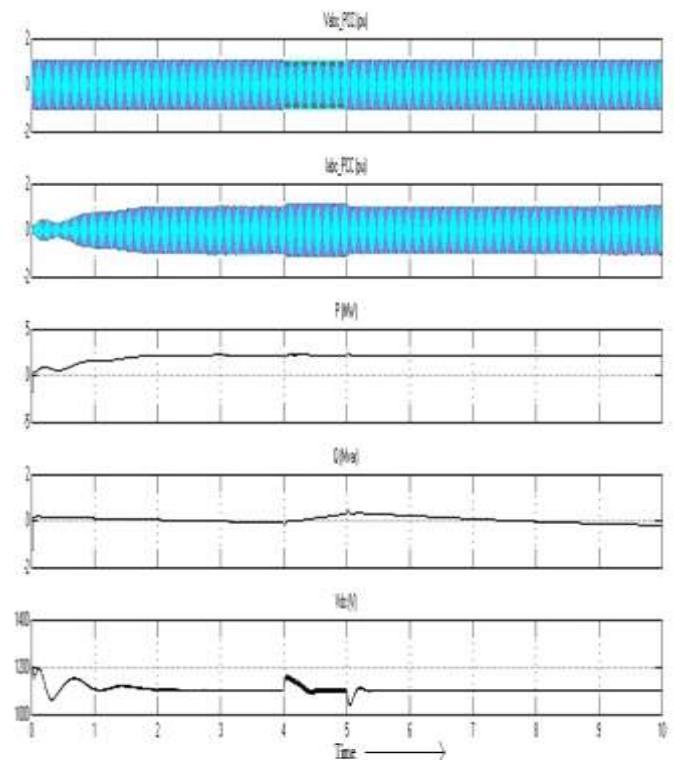


**Fig -6:** Response of the system under the single line to a ground fault condition.

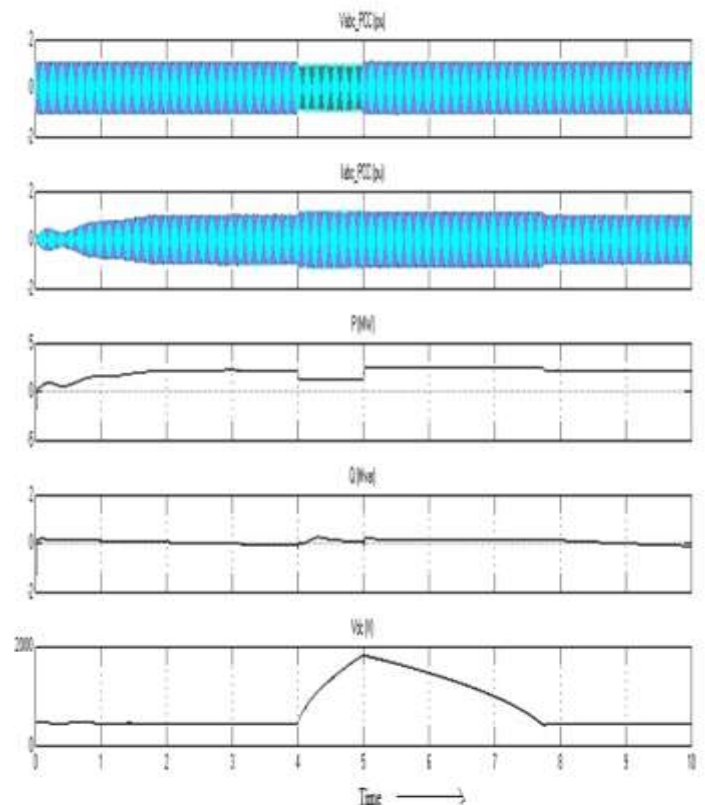


**Fig -7:** Response of the system under line to line fault condition.

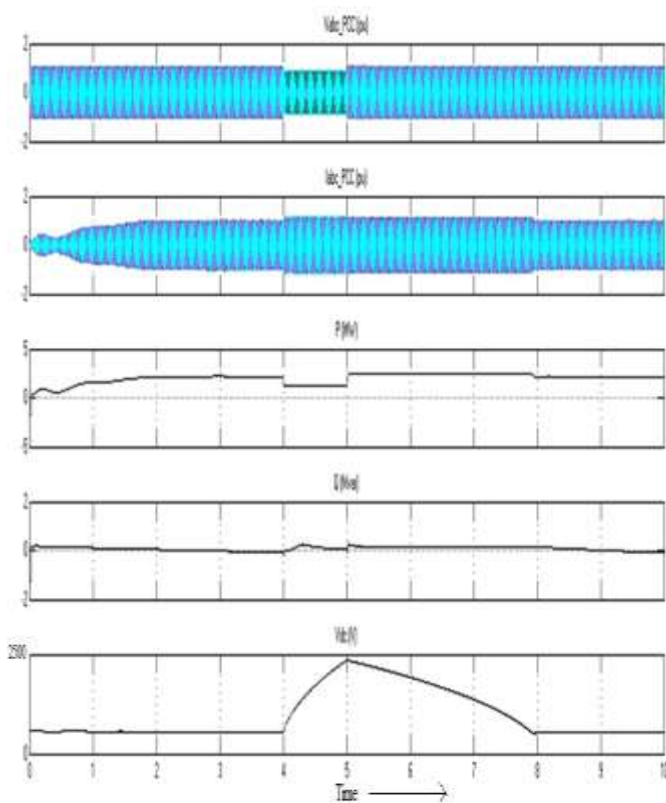


**Fig -8:** Response of the system under the double line to a ground fault condition.

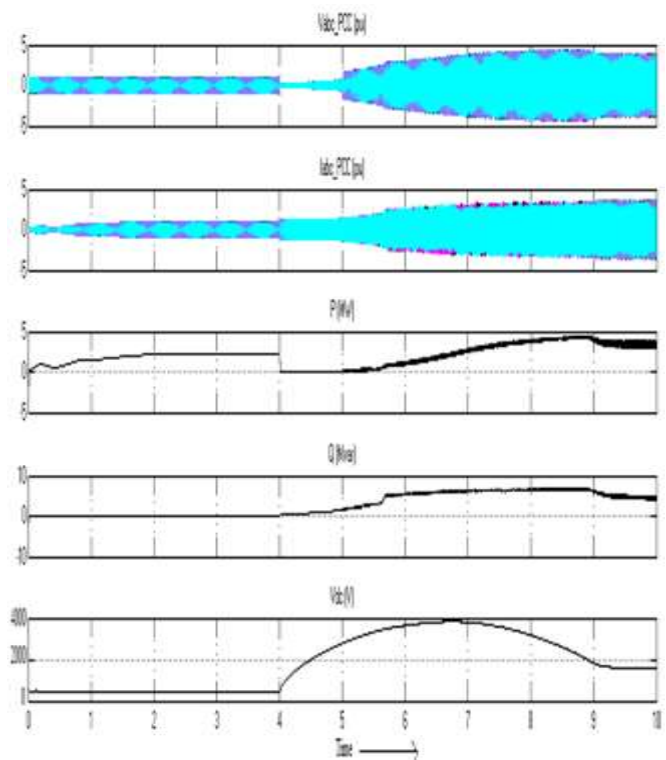


**Fig -9:** Response of the system under three phase fault condition.

**Fig- 8** shows the response of the system under the double line to a ground fault condition. The fault occurred at  $t = 4s$  and cleared at  $t = 5s$ . Active power reference is set at 2 MW and reactive power reference is set at zero. During fault distortion in grid current occurs and thus distortions are seen in active and reactive power. When fault is cleared the active and reactive power follow the respective references. It also shows the effect of double line to ground fault on dc link voltage and voltage and current at the point of common coupling.

**Fig- 9** shows the response of the system under three phase fault condition. The fault occurred at  $t = 4s$  and cleared at  $t = 5s$ . Active power reference is set at 2 MW and reactive power reference is set at zero. During the three phase fault, distortion in grid current occurs and thus distortions are seen in active and reactive power. When fault is cleared the active and reactive power follow the respective references. It also shows the effect of three phase fault on dc link voltage and voltage and current at the point of common coupling.

### 3. CONCLUSION

In this paper, the performance analysis of the Grid Side Converter Control system using FOC algorithm has been examined. Steady-state and dynamic response of the system has been evaluated. The results under various operating conditions show that the system provides a good response. During unbalance of the grid voltage and under different fault conditions the distortion in output current increases significantly. This system provides subsequent accuracy under steady-state and dynamic conditions.

### REFERENCES

- [1] Yassin, H. M., H. H. Hanafy, and Mohab M. Hallouda. "Optimization of PMSG Variable Speed Wind Energy Conversion System Controller Parameter by Biogeography-Based Optimization." *Journal of Electrical Engineering*.
- [2] Verma, J., Tiwari, Y., Mishra, A., & Singh, N. (2014). Performance analysis and simulation of wind energy conversion system connected with grid. *International Journal of Recent Technology and Engineering*, 2(6), 33-38.
- [3] Abdullah, M. A., Yatim, A. H. M., & Tan, C. W. (2011, June). A study of maximum power point tracking algorithms for wind energy system. In *Clean Energy and Technology (CET), 2011 IEEE First Conference on* (pp. 321-326). IEEE.
- [4] Nath, S., & Rana, S. (2011). The modeling and simulation of wind energy based power system using MATLAB. *International Journal of Power System Operation and Energy Management*, 1(2), 12-17.
- [5] Chen, J., Wu, H., Sun, M., Jiang, W., Cai, L., & Guo, C. (2012, May). Modeling and simulation of directly driven wind

turbine with permanent magnet synchronous generator. In Innovative Smart Grid Technologies-Asia (ISGT Asia), 2012 IEEE (pp. 1-5). IEEE.

[6] Chinchilla, M., Arnaltes, S., & Burgos, J. C. (2006). Control of permanent-magnet generators applied to variable-speed wind-energy systems connected to the grid. IEEE Transactions on energy conversion, 21(1), 130-135.

[7] Abir, A., & Mehdi, D. (2017, March). Control of permanent-magnet generators applied to variable-speed wind-energy. In Green Energy Conversion Systems (GECS), 2017 International Conference on (pp. 1-6). IEEE.

[7] Samanvorakij, S., & Kumkratug, P. (2013). Modelling and simulation PMSG based on wind energy conversion system in MATLAB/SIMULINK. In Proc. of Second Intl. Conf. on Advances in Electronics and Electrical Engineering (pp. 37-41).

[8] Rahimi, M., & Parniani, M. (2010). Transient performance improvement of wind turbines with doubly fed induction generators using nonlinear control strategy. IEEE Transactions on Energy Conversion, 25(2), 514-525.

[9] Yang, L., Xu, Z., Ostergaard, J., Dong, Z. Y., & Wong, K. P. (2012). Advanced control strategy of DFIG wind turbines for power system fault ride through. IEEE Transactions on power systems, 27(2), 713-722.

[10] Zoghlami, M., Kharoui, R., Fnaeich, N., & Bacha, F. (2016, June). Direct Power Control strategy for variable speed Wind Energy Conversion System based on PMSM Generator. In Power Electronics, Electrical Drives, Automation and Motion (SPEEDAM), 2016 International Symposium on (pp. 1348-1353). IEEE.

[12] Patel, A. M., & Patel, J. J. PMSG with Inverter using Park's Transformation for Transient Fault Analysis.

[13] Wang, Q., & Chang, L. (2004). An intelligent maximum power extraction algorithm for inverter-based variable speed wind turbine systems. IEEE Transactions on power electronics, 19(5), 1242-1249.

[14] Saidur, R., Islam, M. R., Rahim, N. A., & Solangi, K. H. (2010). A review on global wind energy policy. Renewable and Sustainable Energy Reviews, 14(7), 1744-1762.

[15] Year End Review 2017. Ministry of New and Renewable Energy (MNRE) [Online].

Available:<http://www.eqmagpro.com/year-end-review-2017-mnre>.